Proceedings of the ASME 2018 37th International Conference on Ocean, Offshore and Arctic Engineering
OMAE2018
June 17-22, 2018, Madrid, Spain

OMAE2018-78375

NUMERICAL SIMULATIONS OF SHIP BOW AND SHOULDER WAVE BREAKING IN DIFFERENT ADVANCING SPEEDS

Zhen Ren
Collaborative Innovation Center for Advanced Ship and Deep-Sea Exploration, State Key Laboratory of Ocean Engineering, School of Naval Architecture, Ocean and Civil Engineering, Shanghai Jiao Tong University, Shanghai, China

Jianhua Wang
Collaborative Innovation Center for Advanced Ship and Deep-Sea Exploration, State Key Laboratory of Ocean Engineering, School of Naval Architecture, Ocean and Civil Engineering, Shanghai Jiao Tong University, Shanghai, China

Decheng Wan*
Collaborative Innovation Center for Advanced Ship and Deep-Sea Exploration, State Key Laboratory of Ocean Engineering, School of Naval Architecture, Ocean and Civil Engineering, Shanghai Jiao Tong University, Shanghai, China
*Corresponding author:
dcwan@sjtu.edu.cn

ABSTRACT

The KCS model is employed for the numerical simulations to investigate the wave breaking phenomena of the bow and shoulder wave. RANS approach coupled with high resolution VOF technique is used to resolve the free surface. In order to study the speed effects on the phenomena of ship wave breaking, four different speeds, i.e. *Fr*=0.26, 0.30, 0.32, 0.35, are investigated in calm water. Predicted resistance and wave patterns under *Fr*=0.26 are validated with the available experiment data, and good agreement is achieved. For the *Fr*=0.26 case, the wave pattern is steady, and the alternate variation of vorticity appear near the free surface is associated with the wake field. The breaking wave phenomena can be observed when the Froude number is over 0.32 and the *Fr*=0.35 case shows most violent breaking bow wave. For the *Fr*=0.35 case, the process of overturning and breaking of bow wave is observed clearly, and at the tail of bow wave, some breaking features of free surface are also captured. The reconnection of the initial plunger with the free surface results in a pair of counter-rotating vortex that is responsible for the second plunger and scar.

INTRODUCTION

The phenomena of wave breaking of bow and shoulder waves always occur for high speed surface ships. Breaking waves can strongly affect the resistance performance since it will cost the energy of the ship significantly. Thus, it is of great significance to study the ship breaking waves. Currently, the researches of the ship bow wave breaking mainly relied on the hydrodynamic experiments. In 1997, Dong, et al (1997) studied on the structure of bow waves of the model, DTMB 4817, via ship model towing experiment [1]. They analyzed the bow wave with the mild and steep slope and the three-dimensional structure of the bow wave. Olivieri, et al. (2007) focused on the scars and vortices induced by bow and shoulder wave breaking of DTMB 5415 [2]. The direct correlation was shown between regions of wave slope larger than 17 deg and regions of large rms in wave height variation. Roth, et al (1999) measured the flow structure and turbulence within the bow wave of DDG-51 model 5422 [3]. In the measurements, they found that the wave shape is fairly stable except for the forward face where wave height variations double. These experiments provided the rich and reliable data for the next studies. Noblesse, et al (2013) reviewed the studies before 2013, and analyzed the overturning and breaking bow wave regimes, and the boundary that divided these two flow regimes [4].

With the development of computational fluid dynamics, researchers began to study the wave breaking by utilizing the numerical method since the convenient and accurate way is provided and more detailed information in flow field can be obtained through this method. Wilson, et al (2006) utilized the URANS code, CFDSHIP-IOWA, to study the high-speed transom stern ship ((R/V Athena I)) with breaking waves under different speeds (*Fr* = 0.25, 0.43 and 0.62) [5]. Simonsen, et al

(2014) studied the added resistance of KCS in regular waves. In their study, they presented the relation between the wave parameters, such as encounter frequency, wave length and heading, and bow wave [6]. Marrone, et al (2011) used SPH method to analyze the breaking wave pattern of different fast ships, and they obtained the satisfactory achievement [7]. Marrone, et al (2012) use a 3D parallel SPH model to simulate the ship wave breaking [8]. They compared the results with experiment data and the results From RANS calculations that was combined with the level set method. Wang and Wan (2017) studied the bow wave breaking of DTMB 5415 based on the CFD solver, naoe-FOAM-SJTU [9]. In their study, the induced free surface scar and breaking wave are observed clearly, and the VOF based on RANS method in the study accurately predicted the wake region associated with breaking wave. The phenomenon of wave breaking was observed when the wave slammed on the bottom of stern in the studies (Liu, et al. (2017a, b, c)) on the wave drift forces of DTC [10-12]. Xia and Wan (2017a) studied the effect of wave steepness on wave breaking properties over submerged reef with a 2D simulation by utilizing the viscous flow solver, naoe-FOAM_SJTU [13]. In their studies, the wave breaking and overturning that effected by the wave steepness was mainly investigated. The profile and properties of the wave breaking was clearly depicted in their study (Xia, et al, 2017b) of the hydrodynamic characteristics of floating platform over the submerged terrain [14].

In the present work, the focus is on the bow wave and shoulder breaking of the KCS. The open source software OpenFOAM is used to complete the numerical simulations. In the simulations, RANS approach coupled with high resolution VOF technique is used to resolve the free surface. Validation is conducted at Fr = 0.26. In this paper, the phenomena of ship wave breaking at different speeds, i.e. Fr = 0.26, 0.30, 0.32, 0.35, are investigated in calm water. The resistance, wave pattern and vorticity are analyzed to understand the ship wave breaking and speed effects further.

Numerical method

Governing equations

In the simulations, the governing equations mainly include the mass conservation equation Equation (1) and the momentum equation Equation (2), which can be written as:

The mass conservation equation:

$$\nabla \cdot \mathbf{U} = 0 \tag{1}$$

The moment conservation equation:

$$\frac{\partial \rho \mathbf{U}}{\partial t} + \nabla \cdot \left(\rho(\mathbf{U}-\mathbf{U}_g)\mathbf{U}\right) = -\nabla p_d - \mathbf{g}\cdot\mathbf{x}\nabla\rho + \nabla\cdot(\mu_{eff}\nabla\mathbf{U}) + (\nabla\mathbf{U})\cdot\nabla\mu_{eff} + f_\sigma \tag{2}$$

where $\mathbf{U}$ is fluid velocity field and $\mathbf{U}_g$ is the grid velocity; p_d represents the dynamic pressure; ρ is the mixture density; $\boldsymbol{g}$ is the gravity acceleration; μ_{eff} is effective dynamic viscosity, in which v and v_t are kinetic and eddy viscosity, respectively, and v_t is obtained from turbulence model. f_σ is surface tension term that plays an important role in wave breaking simulation.

The two-equation shear stress transport model, SST k-ω model (Menter, et al, 2003), is selected to solve the Reynolds stress [15]. k denotes turbulence kinetic energy and ω denotes dissipation rate. The turbulence model combines the advantages of the standard k-ε model and k-ω model to make sure that the free surface is not influenced and ensure the accuracy and reliability of the solution at the wall.

VOF method

Here the Volume of Fluid (VOF) method with artificial compression (Weller and Weller, 2008) is used to capture the free surface [16]. Details of the VOF solution procedure as implemented in OpenFOAM are described by Rusche, (2003) [17]. The transport equation is expressed as:

$$\frac{\partial \alpha}{\partial t} + \nabla\cdot\left(\rho(\mathbf{U}-\mathbf{U}_g)\alpha\right) + \nabla\cdot(\mathbf{U}_r(1-\alpha)\alpha) = 0 \tag{3}$$

where α is the volume of the fraction, indicating the relative proportion of fluid in each cell and its value is always between zero and one:

$$\begin{cases} \alpha = 0 & air \\ \alpha = 1 & water \\ 0 < \alpha < 1 & interface \end{cases} \tag{4}$$

In Equation (3), $\mathbf{U}_r$ is the velocity field used to compress the interface, which can simulate the large deformation of free surface. But it takes effect only on the surface interface due to the term (1-α) α. The expression of this term can be found in Berberović (2009) [18].

Computation and Results

Grid Generation

The geometry of KCS model (case2.10, L_{pp}=6.0702m, with rudder) can be obtained in the workshop on CFD in ship hydrodynamics, Tokyo 2015. In the experiments, the model has two degrees of Freedoms, heave and pitch, in waves. In order to simplify the numerical simulations, the hull is fixed in calm water without the sinkage and trim being not taken into consideration.

All-hexahedral unstructured grid is generated by the software, Hexpress. The number of initial mesh that is 80×24×36 in x, y, z direction, is 4 times of the basic number that is default setting. Six refinement regions are adopted to refine the grids around the hull, especially near the bow and shoulder waves, and the free surface. the positions and sizes of the refinement regions are set according to the previous studies and

Kelvin wave pattern. The strategy of refinement is that the grid size of the next level is half the size of the current grid. For example, the refinement level of Bow Wave (Near) is 6, indicating that the size of the region is one-64th of the initial size. The scale of the size of the highest-level refinement region to L_{pp} is about 9.7e-4. Figure 1 shows the computational domain and the boundary conditions. Figure 2 presents the arrangement of refinement regions. The refinement levels are shown in the Table 1. Figure 3 shows the local mesh, such as, the refinement grid of bow wave, hull, bow and rudder.

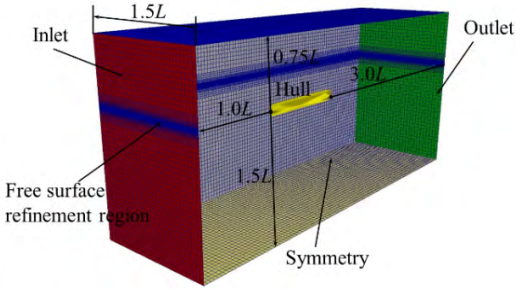

Figure 1 Domain and Boundary conditions.

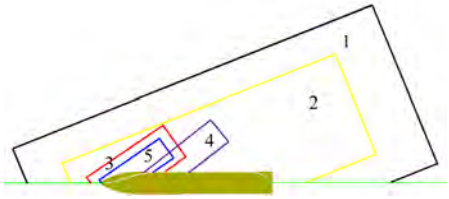

Figure 2 Refinement Regions.

Table 1 Grid dimension

Block Name	No.	Refine level (x, y, z)
Free Surface		0×0×3
Far	1	2×2×2
Near	2	4×4×4
Bow Wave(Far)	3	5×5×5
Shoulder Wave	4	5×5×5
Bow Wave(Near)	5	6×6×6

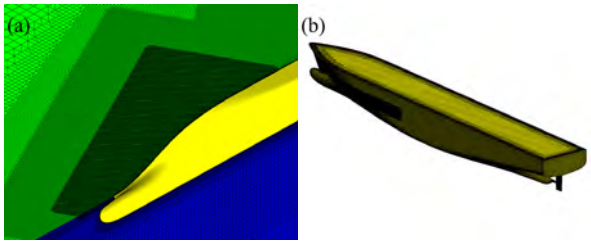

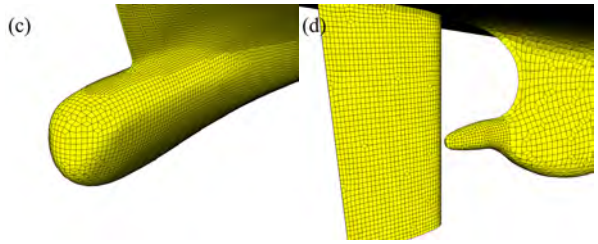

Figure 3 Local Mesh (a: local mesh near bow; b: hull mesh; c: bow mesh; d: rudder mesh).

Validation of Numerical Scheme

The focus of the present study is on the resolution of bow wave breaking of KCS at different speeds, i.e. Fr = 0.26, 0.30, 0.32, 0.35. The condition at Fr = 0.26 is selected to validate the prediction accuracy of the current numerical scheme. Table 2 shows the comparison between the predicted resistance and the experiment data. The sinkage and trim of the hull is not taken into consideration in order to simplify the numerical simulation, so the error of C_t, about -4.5%, is acceptable. Figure 4 shows the wave height of the three profiles (y/L = 0.0741, 0.1509, 0.4224), obtained by experiment and numerical simulations. From the near field to the far field, the calculated free surface is consistent with the experimental measurements. The wave profiles on hull surface achieved by numerical method and experiment data are shown in Figure 5. Except for the deviation of the bow and stern wave, the other results are in good agreement with the experimental measurements. The above results prove that the numerical scheme in the present work is reliable.

Table 2 Comparison of experimental and predicted resistance

Parameters	EFD	CFD
U (m/s)	2.017	2.017
Sinkage ($/L_{pp}$)	-2.074e-3	None
Trim (deg)	-0.1646	None
Wetted surface area with rudder	6.6978	6.7449
C_t	3.835	3.662
Error		-4.5%

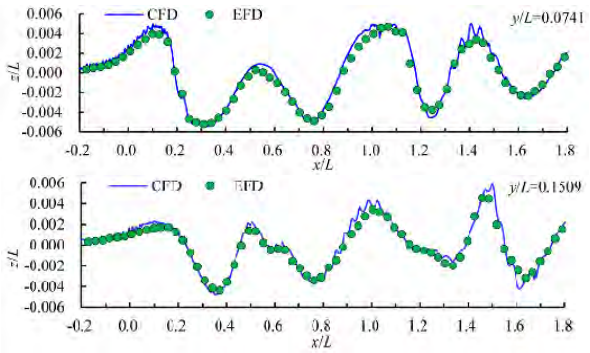

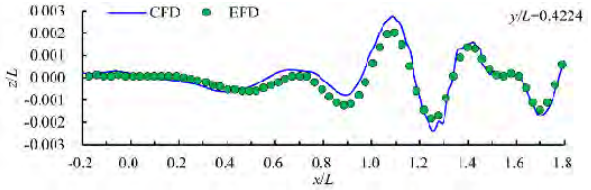

Figure 4 Comparison of Free-surface cuts between experiments (circles) and computational results (line) at different positions.

Resistance under Low Speed

Figure 6 shows predicted frictional, pressure, and total ship resistance for all speeds. The total resistance coefficient, C_t, increases along with the increase of speeds. The trend of frictional resistance coefficient, C_v, is consistent with the total resistance. While the pressure resistance, C_p, decreases along with the increase of speeds. The trends of different resistances components are qualitatively consistent with the results of Wilson, et al (2006) [5].

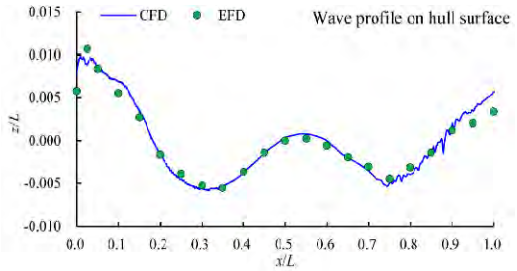

Figure 5 Wave profile on hull surface.

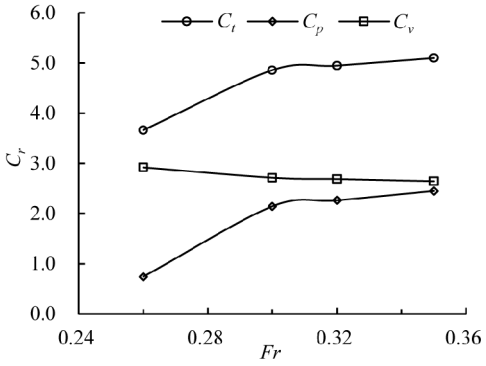

Figure 6 Resistance under different speeds.

Wave Pattern

Figure 7 shows the wave elevation at *Fr*=0.26, 0.30, 0.32 and 0.35. The length and width of bow and shoulder waves for *Fr*= 0.35 case increase obviously than the other conditions. The amplitudes of waves increase rapidly along with the increase of speed.

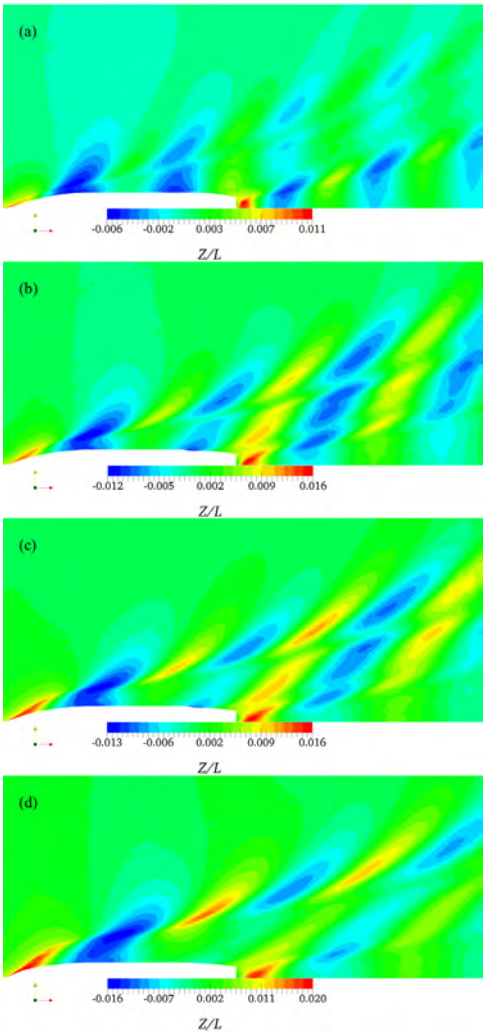

Figure 7 Wave elevation contour at different speeds. (a): *Fr* = 0.26; (b): *Fr* = 0.30; (c): *Fr* = 0.32; (d): *Fr* = 0.35.

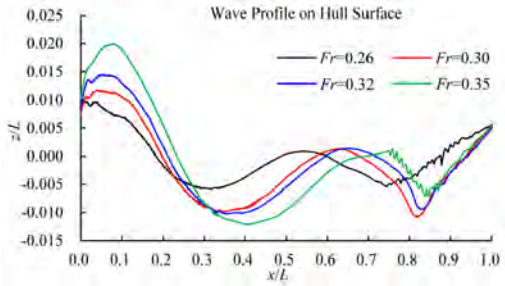

Figure 8 Wave profile on hull surface.

The wave profiles on hull surface are shown in Figure 8. As we can see, there are two crests and troughs of wave on hull surface. The amplitudes of first crests and troughs raise gradually along with the increase of speeds. The variation of second crests is very little among different speeds. The second trough first decreases and then increase along with the increase

of speed. The amplitude of the trough at *Fr*=0.30 is the lowest among the four conditions.

In order to display the bow wave shape more clearly, the local views are presented in Figure 9. At low speed, bow and shoulder wave is quite steady as shown in Figure 9 (a). The shoulder wave can be observed clearly, and its origin is at the point that *x*/*L* is about 0.10 where the shoulder wave separates from the hull downstream. At *Fr*=0.32, a fuzzy outline of bow overturning and scar are shown in Figure 9 (b). But the elevation and thickness of the liquid sheet increase obviously. The overturning and breaking of bow wave can be observed clearly at *Fr* = 0.35, as depicted in Figure 9 (c). The overturning

of bow wave occurs followed by the plunger and breaking tail. In the process of the bow wave overturning, a scar is formed since the plunger reconnects with the free surface.

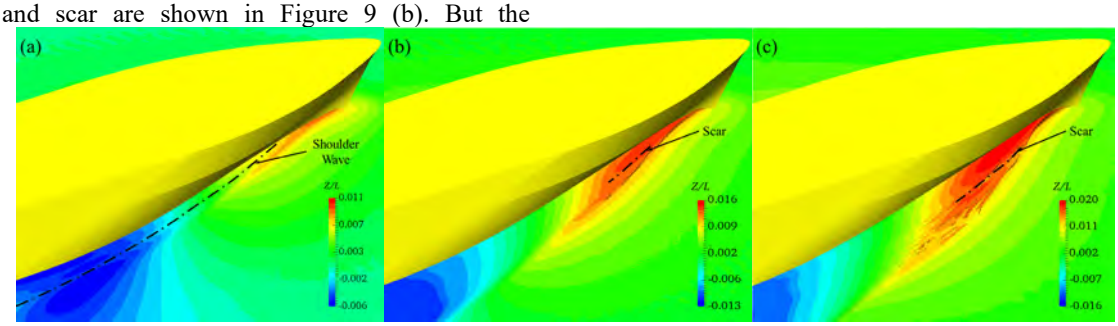

Figure 9 Bow wave under different speeds. (a): *Fr*=0.26; (b): *Fr*=0.32; (c): *Fr*=0.35.

Vorticity Field

Figure 10 reveals the evolution of axial vorticity cross sectional planes at *Fr* = 0.26, 0.35. Overall, the figure clearly indicates many pairs of counter-rotating vortices induced by the bow wave. As shown in Figure 10 (a), for *Fr* = 0.26 case, the axial vorticity that gradually weakens downstream is associated with bow and shoulder wave. V1 and V3 are negative and associated with the first trough and the trough of shoulder wave, respectively. V2 and V4 are positive and associated with the crest of shoulder and bow wave, respectively. Figure 10 (b) displays the distribution and evolution of axial vorticity at *Fr* = 0.35. V1 is negative and associated with the initial plunger. When the initial plunger reconnects with the free surface, a counter-rotating vortex pair (labeled as vortex V2 and V3) is generated. This vortex pair has a rotational orientation that pumps fluid outboard at the toe and is responsible for the formation of the second plunger. Although the second plunger is not observed clearly since the wave breaking occurs, the vorticity (labeled as V4) is generated and has the opposite rotational orientation of V3. V5 and V6 is a pair of counter-rotating vortex and associated with the shoulder wave. The positive vorticity (V6) is generated at the crest of shoulder wave while at the toe, the negative vorticity (V5) is generated.

The axial vorticity contours and cross plane vectors at *x*/*L* =0.2 and *Fr* =0.26 are shown in Figure 11(a). As shown in the figure, the variation of vorticity mainly concentrates near the free surface where the positive and negative vorticity appears alternately. Negative vorticity (V1), corresponding to the first trough, is generated as the ship blocks the inflow and the liquid sheet flows outboard during ship's advancement. And the trend of velocity vector is clockwise as shown in Figure 11 (b). Due to the lag of flow, a bulge that is the shoulder wave is formed outside of the first trough. Positive vorticity (V2) is generated at the crest of shoulder wave where the flow is counter-clockwise and first strengthens and then weakens downstream. Negative vorticity (V3 as shown in Figure 11 (c)) occurs and weakens downstream at the toe where the flow direction is clockwise and

a pair of counter-rotating vorticity (V2 and V3) is formed. V4 is associated with the bow wave and the steepness of bow wave crest weakens gradually with intensity of vorticity decreasing downstream.

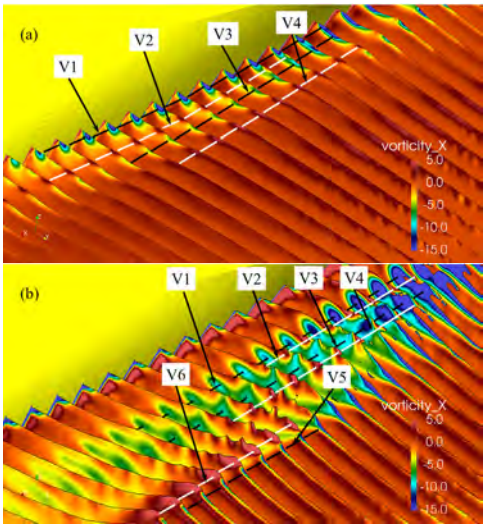

Figure 10 Evolution of axial vorticity downstream. (a): *Fr*=0.26; (b): *Fr*=0.35.

The liquid fleet is formed due to the block effect of ship on the inflow. Under the interaction of gravity and inertial forces, the initial plunger has already formed at *x*/*L* = 0.065, as

shown in Figure 12 (a). The plunger is falling towards the free surface below that results in large differences in the cross-plane velocity vectors in the plunger and the free surface below. The negative axial vorticity (V1) is generated in the high curvature region of the overturning wave. Figure 12 (b) shows the mechanism for the generation of the second plunger. When the falling plunger reconnects with the free surface below, a pair of counter-rotating vortex (V2 and V3) is generated where the orientation of velocity vector is opposite. The counter-rotating vortex is responsible for the second plunger that is not visible clearly for the *Fr* =0.35 case and a scar is formed near V2.

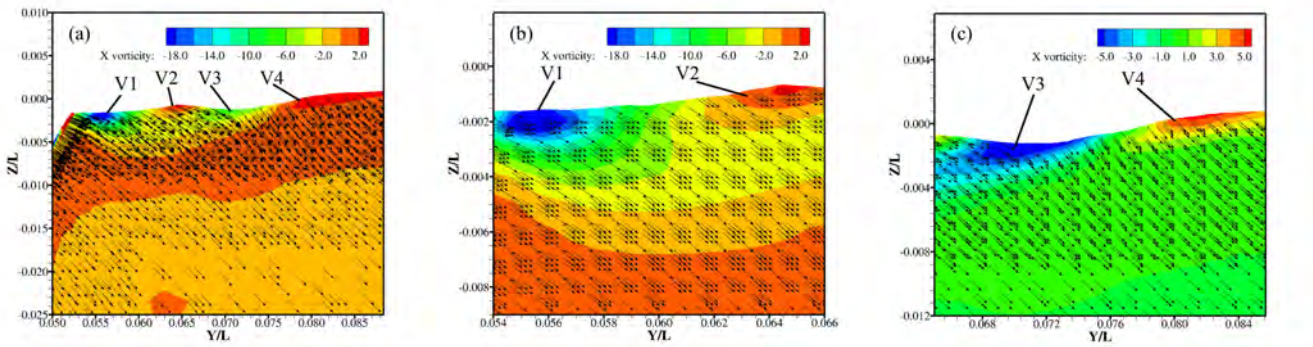

Figure 11 (a) Axial vorticity contours and cross plane vectors at x/L = 0.20 and Fr = 0.26. Magnified portion of vorticity and velocity field in the near (b) and far (c) flow field.

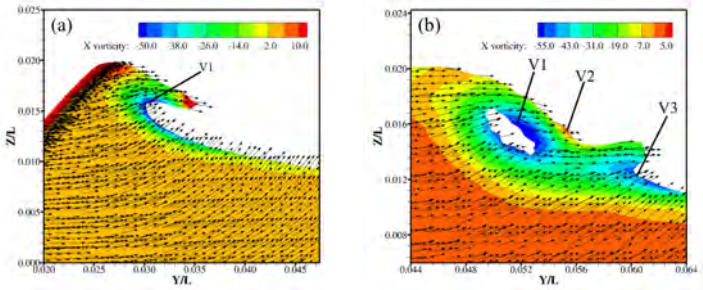

Figure 12 Axial vorticity contours and cross plane vectors at (a): x/L = 0.065, (b): x/L = 0.10, Fr = 0.35.

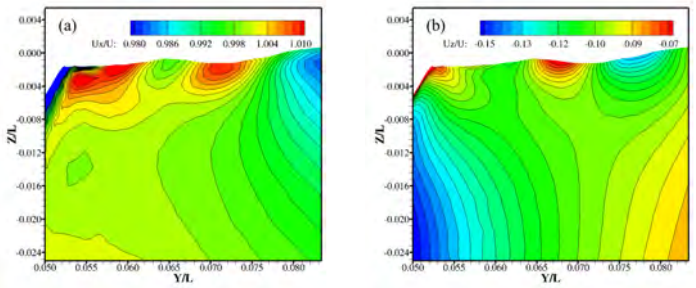

Figure 13 Wake field distribution at x/L = 0.20 and Fr = 0.26. (a): axial velocity and (b): vertical velocity.

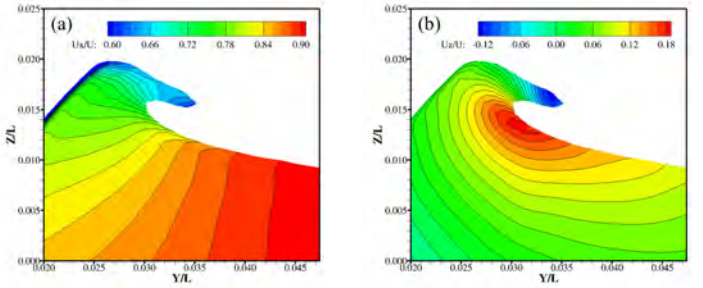

Figure 14 Wake field at x/L = 0.065 and Fr = 0.35. (a): axial velocity; (b): vertical velocity.

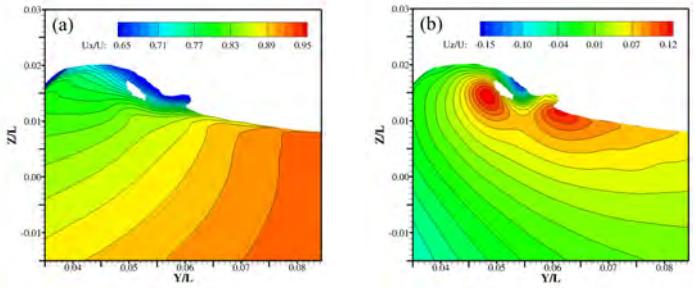

Figure 15 Wake field at x/L = 0.10 and Fr = 0.35. (a): axial velocity; (b): vertical velocity.

Wake Field

The variation of axial and vertical wake field at x/L = 0.20 and Fr = 0.26 near the free surface is shown in Figure 13. The first trough associated with negative vorticity (V1) is an axial low speed region (as shown in Figure 13 (a)) except the region around the hull. Connected with the low speed region, there are two high-speed regions that can be divided into two parts. The interaction between first trough and shoulder wave makes the axial velocity increase in the horizontal region; the axial

velocity below the trough increase due to the three-dimensional effect and the exclusion of the trough on the flow. Near the crest of shoulder wave, at y/L = 0.065, the axial velocity is relatively low, and the vertical velocity is also quite low that its direction is negative as shown in Figure 13 (b).

Figure 14 shows the axial and vertical velocity distribution of the initial plunger at x/L = 0.065 and Fr = 0.35. As shown in Figure 14 (a), the axial velocity gradually increases outboard but in the plunger, the axial velocity is quite low, about 0.6U. The positive vertical velocity increases significantly, about 0.18U, at the toe of the overturning wave while the negative velocity at the tip of the plunger is about 0.12U. The downward movement induced by the gravity causes the reconnection of the initial plunger with the free surface below. The upward movement should be responsible for the negative vorticity.

The wake field at x/L = 0.10 and Fr = 0.35 is shown in Figure 15. The axial velocity increases downward and outboard as shown in Figure 15 (a). The low axial velocity, about 0.65U, mainly focuses in the plunger. When the initial plunger reconnects with the free surface below, the positive vertical velocity region is mainly concentrated at the toe of the initial plunger and second plunger that is not observed clearly. A pair of opposite vertical velocity (as shown in Figure 15 (b)) is observed where the positive is near the scar and the negative is at the toe of second plunger. The opposite velocity is associated with the counter-rotating vortex pair (as shown in Figure 12 (b)).

CONCLUSION

In the present work, an exploratory study of KCS under high speed is performed to study the bow and shoulder wave breaking, to analyze the wave pattern of KCS under high speed and the vorticity and wake fields. The Fr = 0.26 case is utilized to verify the accuracy of the numerical method. The calculated results are in good agreement with the experiment data. The variation of vorticity and wave field is mainly concentrated near the free surface. At Fr = 0.26, two pairs of vorticity appearing on the free surface alternate with positive and negative values and weaken downstream. The appearance of vorticity corresponds to the crest and trough of bow and shoulder wave. At Fr = 0.35, the vorticity develops further from the free surface. Similar to the low speed, the counter-rotating vortex appears and is associated with the wake field where the vertical velocity alternates with positive and negative values. The counter-rotating vortex is responsible for the second plunger, while the initial plunger is formed due to the gravity and inertial forces when the hull blocks the inflow.

Future work of the application is aimed at overcoming the limitation discovered in the present study. The present results show that the present grid distribution is not fine enough to capture the flow field details, such as, the plunging, overturning, in the bow and shoulder waves. So, the more reasonable and refined grid distribution will be adopted to simulate the bow wave breaking of KCS at higher speed, for example, Fr = 0.40, 0.42. In addition, due to the simplification in the present work, the sinkage and trim of the model is not taken into consideration. The numerical simulations of bow and shoulder wave breaking of KCS with six degrees of freedom will be conducted in the future work. Even though the phenomenon of bow wave breaking is captured, some small-scale features, such as, air entertainment, capillary wave, are not presented through the present study. So, the effort should be made in these aspects.

ACKNOWLEDGMENTS

This work is supported by the National Natural Science Foundation of China (51490675, 11432009, 51579145), Chang Jiang Scholars Program (T2014099), Shanghai Excellent Academic Leaders Program (17XD1402300), Program for Professor of Special Appointment (Eastern Scholar) at Shanghai Institutions of Higher Learning (2013022), Innovative Special Project of Numerical Tank of Ministry of Industry and Information Technology of China (2016-23/09) and Lloyd's Register Foundation for doctoral student, to which the authors are most grateful.

REFERENCES

[1] Dong, R., Katz, J., Huang, T. 1997, "On the structure of bow waves on a ship model," *Journal of Fluid Mechanics,* Vol. 346, pp. 77-115.

[2] Olivieri, A., Pistani, F., Wilson, R., Campana, E. F., Stern, F. 2007, "Scars and Vortices Induced by Ship Bow and Shoulder Wave Breaking," *Journal of Fluids Engineering,* Vol. 129, pp. 1445-1459.

[3] Roth, G. I., Mascenik, D. T., Katz, J. 1999, "Measurements of the flow structure and turbulence within a ship bow wave," *Physics of Fluids,* Vol. 11, pp. 3512-3523.

[4] Noblesse, F., Delhommeau, G., Liu, H., Wan, D. C., Yang, C. 2013, "Ship bow waves," *Journal of Hydrodynamics,* Vol. 25, pp. 491-501.

[5] Wilson, R. V., Carrica, P. M., Stern, F. 2006, "URANS simulations for a high-speed transom stern ship with breaking waves," *International Journal of Computational Fluid Dynamics,* Vol. 20, pp. 105-125.

[6] Simonsen, C. D., Otzen, J. F., Nielsen, C., Stern, F. 2014, "CFD prediction of added resistance of the KCS in regular head and oblique waves," *30th Symposium on Naval Hydrodynamics,* Hobart, Australia.

[7] Marrone, S., Colagrossi, A., Antuono, M., Lugni, C., Tulin, M.P. 2011, "A 2D+t SPH model to study the breaking wave pattern generated by fast ships," *Journal of Fluids and Structures,* Vol. 27, pp. 1199-1215.

[8] Marrone, S., Bouscasse, B., Colagrossi, A., Antuono, M. 2012, "Study of ship wave breaking patterns using 3D

parallel SPH simulations," *Computers & Fluids,* Vol. 69, pp. 54-66.

[9] Wang, J. H., Wan, D. C. 2017, "Breaking Wave Simulations of High-speed Surface Combatant using OpenFOAM," *Proceedings, 8th International Conference on Computational Methods,* Guilin, Guangxi, China, pp. 841-852.

[10] Liu, C., Wang, J. H., Wan, D. C., Yu, X. G., 2017a, "Computation of Wave Drift Forces and Motions for DTC Ship in Oblique Waves," *Proceedings, 27th International Ocean and Polar Engineering Conference,* San Francisco, California, USA, pp. 144-152.

[11] Liu, C., Wang, J. H., Wan, D. C. 2017b, "Computation of wave drift forces and motions for DTC ship in oblique waves," *Proceedings, 14th National Conference of Hydrodynamics,* Changchun, China, pp. 1374-1382.

[12] Liu, C., Wang, J. H., Wan, D. C. 2017c, "The Numerical Investigation on Hydrodynamic Performance of Twisted Rudder during Selfpropulsion," *Proceedings, the 8th International Conference on Computational Methods*, Guilin, Guangxi, China, pp. 934-943.

[13] Xia, K., Wan, D. C. 2017a, "Effects of wave steepness on wave breaking properties over submerged reef," *Proceedings, the 8th International Conference on Computational Methods*, Guilin, Guangxi, China, pp. 952-961.

[14] Xia, K., Ai, Y., Wan, D. C. 2017b, "Hydrodynamic Study of Wave Evolution Characteristics around Semi-submersible Platform in Shallow Water with Submerged Terrain near Island," *Proceedings, the 27th International Ocean and Polar Engineering Conference,* San Francisco, California, USA, pp. 161-169.

[15] Menter, F. R., Kuntz, M., Langtry, R. 2003, "Ten years of industrial experience with the SST turbulence model, Turbulence," *Heat and Mass Transfer*, Vol. 4, pp. 625-632.

[16] Weller, H., Weller, H. 2008, "A high-order arbitrarily unstructured finite-volume model of the global atmosphere: Tests solving the shallow-water equations," *International Journal for Numerical Methods in Fluids,* Vol. 56, pp. 1589-1596.

[17] Rusche, H. 2003, "Computational fluid dynamics of dispersed two-phase flows at high phase fractions," Ph.D. Thesis. Imperial College London, London, UK.

[18] Berberović, E., Hinsberg, N.P., Jakirlić, S., Roisman, I.V., Tropea, C. 2009, "Drop impact onto a liquid layer of finite thickness: Dynamics of the cavity evolution," *Physical Review,* E 79, 036306.